The Astrophysical Journal, 909:107 (12pp), 2021 March 10 https://doi.org/10.3847/1538-4357/abdc27

Rigorous Theory for Secondary Cosmic-Ray Ionization

Alexei V. Ivlev[1], Kedron Silsbee[1], Marco Padovani[2], and Daniele Galli[2]
[1] Max-Planck-Institut für Extraterrestrische Physik, 85748 Garching, Germany; ivlev@mpe.mpg.de
[2] INAF–Osservatorio Astrofisico di Arcetri, Largo E. Fermi 5, I-50125 Firenze, Italy
Received 2020 November 17; revised 2021 January 6; accepted 2021 January 13; published 2021 March 10

Abstract

The energy spectrum of electrons produced in molecular gas by interstellar cosmic rays (CRs) is rigorously calculated as a function of gas column density N traversed by the CRs. This allows us to accurately compute the local value of the secondary ionization rate of molecular hydrogen, $\zeta_{\rm sec}(N)$, as a function of the local primary ionization rate, $\zeta_p(N)$. The ratio $\zeta_{\rm sec}/\zeta_p$ increases monotonically with N, and can considerably exceed the value of $\approx$0.67 commonly adopted in the literature. For sufficiently soft interstellar spectra, the dependence $\zeta_{\rm sec}/\zeta_p$ versus N is practically insensitive to their particular shape and thus is a general characteristic of the secondary CR ionization in dense gas.

Unified Astronomy Thesaurus concepts: Secondary cosmic rays (1438); Molecular clouds (1072)

1. Introduction

The ionization of dense gas by cosmic rays (CRs) is a problem of fundamental importance in astrophysics and astrochemistry. Being the dominant source of ionization (McKee 1989; Caselli et al. 1998; Neufeld & Wolfire 2017) and UV emission (Prasad & Tarafdar 1983) in dark regions, low-energy CRs govern the evolution of molecular clouds and the formation of stars (Caselli & Ceccarelli 2012; Padovani et al. 2020). The processes induced by CRs affect both the chemistry (Keto & Caselli 2008; Keto et al. 2014) and thermodynamics (Galli et al. 2002; Glassgold et al. 2012; Ivlev et al. 2019) of the clouds. Furthermore, the level of ionization controls the degree to which the gas is coupled to the magnetic field (Shu et al. 1987), which has profound implications for properties of disks around young stars (Zhao et al. 2016, 2018).

CRs interacting with the gas generate electron-ion pairs, with electrons having sufficient energy to produce further ionization. These processes of primary and secondary ionization are characterized by the respective ionization rates (the number of ionizations per unit time and per gas particle), ζ_p and $\zeta_{\rm sec}$. While ζ_p can be straightforwardly derived for a given CR spectrum, computing $\zeta_{\rm sec}$ is a much more subtle task. Dalgarno & Griffing (1958) first calculated the ratio $\zeta_{\rm sec}/\zeta_p$ for monoenergetic protons in atomic hydrogen, finding a value of $\approx$0.67 for proton energies above a few megaelectronvolts. This value was later adopted by Spitzer & Tomasko (1968) and other authors as a constant multiplicative factor for an interstellar proton spectrum. For monoenergetic protons interacting with molecular hydrogen, Glassgold & Langer (1973) found $\zeta_{\rm sec}/\zeta_p$ increasing from 0.23 to 0.54 for energies between 1 and 10 MeV, while Cravens & Dalgarno (1978) reported ratios from 0.44 to 0.74 for energies between 1 and 100 MeV.

In the present paper, we rigorously compute the energy spectrum of electrons that are produced by interstellar CRs penetrating dense astrophysical objects (such as molecular clouds or circumstellar disks), and derive the resulting rate of secondary ionization as a function of the gas column density. We point out that knowing the exact spectrum of secondary electrons makes it possible to accurately evaluate characteristics of other important processes driven by CRs, such as the local rates of gas heating and H_2 dissociation, as well as the local magnitude of the UV field due to H_2 fluorescence.

Unlike the approach by Dalgarno & Griffing (1958; and similar approaches by Knipp et al. 1953 and Erskine 1954), aimed at calculating the average number of ion pairs, we obtain a balance equation describing the steady-state electron spectrum, which is similar to the degradation equation by Spencer & Fano (1954). To the best of our knowledge, this is the first attempt to accurately compute the secondary electron spectrum produced by CRs. Previous attempts (e.g., by Spencer & Fano 1954; Xu & McCray 1991) were focused on numerically calculating the spectral degradation of monoenergetic electrons. Furthermore, most astrophysical applications addressed the interaction of CRs with atomic or partially ionized low-density and low-column density gas, while applications to dense gas neglected any dependence of $\zeta_{\rm sec}/\zeta_p$ on the column density. We show that this ratio is not a constant, but increases with the column traversed by CRs, and that its magnitude can considerably exceed the commonly adopted value of $\approx$0.67. It is worth noting that our approach can be easily generalized to compute secondary X-ray ionization.

2. Definitions and Assumptions

The energy distribution of CR species is characterized by their spectrum $j(E)$, which has the dimensions of a differential flux per unit energy and solid angle ($\rm cm^{-2}\,s^{-1}\,eV^{-1}\,sr^{-1}$) and depends on the kinetic energy E. We are interested in calculating the ionization rate of molecular hydrogen. The ionization is assumed to be due to interstellar CR protons; the contribution of interstellar electrons can be neglected (see discussion in Section 4.4). Protons with the local (attenuated) spectrum $j_p(E, N)$ produce primary ionization of H_2, occurring at the gas column density N at a rate of $\zeta_p(N)$. This generates *secondary electrons* with the local spectrum $j_{\rm sec}(E, N)$, leading to secondary ionization of H_2 at a rate of $\zeta_{\rm sec}(N)$. Adding heavier CR nuclei with the interstellar spectrum proportional to that of protons introduces a negligible contribution to the dependence $\zeta_{\rm sec}/\zeta_p$ versus N (see Section 6). For the sake of clarity, $j_{\rm sec}$ is calculated neglecting ionization of helium and heavier gas species, but our approach is applicable in general to

arbitrary gas composition. The gas is assumed to be neutral, because the effect of Coulomb collisions is vanishingly small for the ionization fractions expected in dense clouds (see Section 4.5).

We would like to stress that the definition of "primary electrons" adopted in the literature often refers to the *first* generation of electrons produced by CRs. In fact, the self-consistent treatment (Spencer & Fano 1954) does not make any distinction between electrons' generations, and therefore *all* produced electrons should be treated as secondary.

2.1. Differential Ionization Cross Sections

The primary and secondary ionization of gas species are generally characterized by the respective differential cross sections, $\partial\sigma_p/\partial\varepsilon$ and $\partial\sigma_e/\partial\varepsilon$, which are functions of E and ε. The cross sections determine the probability that a proton (p) or electron (e) of energy E produces an ejected electron of energy ε.

For proton impact ionization, we adopt the following approximate expression (Rudd 1987, 1988; Rudd et al. 1992):

$$\frac{\partial\sigma_p}{\partial\varepsilon}(E,\,\varepsilon) \approx \frac{f_p(E)}{(1+\tilde{\varepsilon})^3}\left[\tilde{\varepsilon} + \eta_p \ln\left(\frac{m_e}{m_p}\tilde{E}\right)\right], \tag{1}$$

where $\tilde{E} = E/I$ and $\tilde{\varepsilon} = \varepsilon/I$ denote the energy normalization by the ionization potential I, and $f_p(E) \propto E^{-1}$. The first term in the brackets represents the contribution of binary proton–electron collisions, while the logarithmic term with the prefactor η_p characterizes the dipole contribution from the Bethe theory (Bethe 1930; Landau & Lifshitz 1991), arising due to dominant small-momentum transfer in inelastic collisions with a molecule.

It must be stressed that in Equation (1), we use the expression valid for $\tilde{E} \gg m_p/m_e$, i.e., we assume that the proton energy is much larger than 3×10^4 eV: as shown in Section 3, the primary ionization at column densities over $\sim10^{20}\,\mathrm{cm}^{-2}$ is determined by protons with energies much higher than this value. Hence, the accuracy of Equation (1) is completely sufficient for the purposes of our studies.

The value of η_p varies a little from one literature source to another. For the ionization of molecular hydrogen, Equation (11) in Rudd (1987) gives $0.791/0.917 = 0.863$; Equation (10) with Table 1 in Rudd (1988) suggests $0.80/1.06 = 0.755$; and Equations (43)–(48) with Table 5 in Rudd et al. (1992) give $0.96/1.04 = 0.923$. In this paper, we adopt the latter value.

The differential cross section for the electron-impact ionization takes into account exchange effects. In this case, we generally write (Kim & Rudd 1994; Kim et al. 2000)

$$\frac{\partial\sigma_e}{\partial\varepsilon}(E,\,\varepsilon) = f_e(E)[\varphi_{\rm M}(\varepsilon,\,\varepsilon') + \eta_e \ln\tilde{E}\;\varphi_{\rm dip}(\varepsilon,\,\varepsilon')], \tag{2}$$

where ε and $\varepsilon' = E - \varepsilon - I$ are energies of two electrons produced by impact of an electron with energy E. The function $f_e(E)$, given by the first factor of Equation (3) in Kim et al. (2000) multiplied by $2/(1+\eta_e)$, varies as $f_e \propto E^{-1}$ for $E \gg I$. The first term in the brackets describes binary electron–electron collisions according to the modified Mott's formula (Mott 1930; Landau & Lifshitz 1991),

$$\varphi_{\rm M}(\varepsilon,\,\varepsilon') = \frac{1}{(1+\tilde{\varepsilon})^2} + \frac{1}{(1+\tilde{\varepsilon}')^2} - \frac{1}{(1+\tilde{\varepsilon})(1+\tilde{\varepsilon}')}. \tag{3}$$

The function $\varphi_{\rm dip}(\varepsilon,\,\varepsilon')$ is determined by the differential dipole oscillator strength of a molecule. For this paper, we use a symmetrized expression suggested by Kim et al. (2000)

$$\varphi_{\rm dip}(\varepsilon,\,\varepsilon') = \frac{1}{(1+\tilde{\varepsilon})^3} + \frac{1}{(1+\tilde{\varepsilon}')^3}. \tag{4}$$

The prefactor $\eta_e = Q/(2-Q)$ is expressed via a dipole constant Q, a functional of the oscillator strength (see Kim & Rudd 1994). The simple form of Equation (4) is suggested to be used in cases where no reliable data on the oscillator strength are available. Generally, $\varphi_{\rm dip}(\varepsilon,\,\varepsilon')$ is approximated by a (symmetrized) polynomial of $(1+\tilde{\varepsilon})^{-n}$ with $n \geqslant 3$ (Kim & Rudd 1994; Kim et al. 2000), which can be straightforwardly included in our theory.

The value of η_e appears to be less constrained than η_p. Kim & Rudd (1994) and Kim et al. (2000) suggest to set $Q = 1$ ($\eta_e = 1$) when no data are available for a given gas species; at the same time, for hydrogen atoms, they give $Q = 0.5668$ ($\eta_e \approx 0.4$). On the other hand, our calculations in Section 6 show that the ratio $\zeta_{\rm sec}/\zeta_p$ is insensitive to η_e, and therefore we set $\eta_e = 1$.

The use of relativistic expressions for the differential cross sections does not affect the principal results reported in the paper. In particular, calculations with a relativistic formula for the electron-impact ionization (Kim et al. 2000) leave almost unchanged the value of $\zeta_{\rm sec}/\zeta_p$ (see Section 6), leading to its slight increase by less than 2% at the largest analyzed column densities. Thus, for the sake of convenience, we can employ nonrelativistic Equations (1) and (2), even though the high-energy tail of secondary electrons may become relativistic for large columns.

2.2. Ionization Cross Sections

They are obtained by integrating the respective differential cross sections over a range of possible ejected energies. For primary ionization, Equation (1) is integrated from 0 to

$$\varepsilon_{{\rm max},p} = 4\frac{m_e}{m_p}E - I, \tag{5}$$

the maximum energy that can be transferred by a proton of energy E to the ejected electron. Since Equation (1) is applicable for proton energies such that $\varepsilon_{{\rm max},p} \gg I$, we extend the integration to infinity (thus omitting terms going beyond the assumed applicability). This gives the following approximate expression:

$$\sigma_{{\rm ion},p}(E) \approx \frac{1}{2}f_p(E)I\left[1 + \eta_p \ln\left(\tfrac{m_e}{m_p}\tilde{E}\right)\right], \tag{6}$$

valid for $\tilde{E} \gg m_p/m_e$. For the electron-impact ionization, we integrate Equation (2) up to

$$\varepsilon_{{\rm max},e} = \frac{1}{2}(E - I), \tag{7}$$

the maximum value of ε for indistinguishable electrons. This yields the following general formula:

$$\sigma_{\mathrm{ion},e}(E) = f_e(E) I\left[1 - \frac{1}{\tilde{E}} - \frac{\ln \tilde{E}}{1+\tilde{E}} + \frac{\eta_e}{2}\left(1 - \frac{1}{\tilde{E}^2}\right)\ln \tilde{E}\right], \quad (8)$$

valid for any $E \geqslant I$.

3. Local Spectrum of CR Protons

Let us start with a rigorous derivation of the steady-state kinetic equation for CR protons. Assuming their free-streaming propagation (see Padovani et al. 2020, and references therein), the *local* spectrum $j_p(E, N, \mu)$ of protons with pitch-angle cosine μ at column density N is determined by a balance of advection and energy losses:

$$\mu \frac{\partial j_p}{\partial N} + \mathcal{P} - \mathcal{D} = 0. \quad (9)$$

The rates $\mathcal{P}(E)$ and $\mathcal{D}(E)$ at which ionizing collisions of protons lead, respectively, to population and depopulation of their energy state E (we do not indicate dependence on N and μ for brevity) have the form introduced by Fano (1953) and Spencer & Fano (1954):

$$\mathcal{P}(E) = \int_0^{\varepsilon^*_{\mathrm{max},p}} \frac{\partial \sigma_p}{\partial \varepsilon}(E + \varepsilon + I, \varepsilon) j_p(E + \varepsilon + I)\, d\varepsilon, \quad (10)$$

$$\mathcal{D}(E) = j_p(E)\int_0^{\varepsilon_{\mathrm{max},p}} \frac{\partial \sigma_p}{\partial \varepsilon}(E, \varepsilon) d\varepsilon \equiv \sigma_{\mathrm{ion},p}(E) j_p(E), \quad (11)$$

where $\varepsilon_{\mathrm{max},p}$ is given by Equation (5), while $\varepsilon^*_{\mathrm{max},p}$ is obtained from Equation (5) by replacing E with $E + \varepsilon^*_{\mathrm{max},p} + I$. We note that pitch angles of protons remain practically unchanged after ionizing collisions, and therefore Equations (10) and (11) involve only integration over ε. In Appendix A we show that, due to the presence of the small parameter $4(m_e/m_p)$, the difference $\mathcal{P} - \mathcal{D}$ can be written in a differential form. With the accuracy $O(m_e/m_p)$, this leads to the standard kinetic equation in the continuous slowing-down approximation (e.g., Fano 1953; Padovani et al. 2018b),

$$\mu \frac{\partial j_p}{\partial N} + \frac{\partial}{\partial E}(L_p j_p) \approx 0, \quad (12)$$

where $L_p(E)$ is the ionization loss function of protons, given by Equation (A5).

In fact, the proton spectrum is attenuated due to ionization and other mechanisms of continuous losses (such as excitation), and then different contributions are simply summed in Equation (12). For a gas composed of multiple species, the loss function is a sum of the respective partial contributions.

Equation (12) can be generally solved by the method of characteristics. The solution is determined by the proton stopping range,

$$R_p(E) = \int_0^E \frac{dE'}{L_p(E')}, \quad (13)$$

and can be explicitly derived for a power-law form of the interstellar (isotropic) spectrum, $j_p^{\mathrm{IS}}(E)$; see Appendix B. An important parameter applied in the analysis below is the proton attenuation energy $E_{\mathrm{att}}(N)$, which is the inverse function of the stopping range,[3]

$$R_p(E_{\mathrm{att}}) = N. \quad (14)$$

Using a power-law approximation for the loss function of protons, Equation (B2), their attenuation energy for $10^{20}\,\mathrm{cm}^{-2} \lesssim N \lesssim 10^{25}\,\mathrm{cm}^{-2}$ is approximated to within 2% by

$$E_{\mathrm{att}}(N) \approx 2.2\, N_{21}^{0.55}\,\mathrm{MeV}, \quad (15)$$

where N_{21} is the gas column density in units of $10^{21}\,\mathrm{cm}^{-2}$. Equation (15) is obtained assuming the interstellar medium (ISM) composition by Wilms et al. (2000) with hydrogen in the molecular form. Here and below, N denotes the column density of all gas species, related to the H_2 column density via $N \approx 1.20 N_{\mathrm{H_2}}$.

In what follows, the local spectrum of CR protons is calculated from the continuous slowing-down approximation, Equation (12). Padovani et al. (2018b) showed that this approximation becomes increasingly inaccurate around the column density of $N = 10^{25}\,\mathrm{cm}^{-2}$ and above, due to the growing effect of nuclear collisions accompanied by pion production. Therefore, in the present paper, the maximum column used for calculations is set to this value. For the interstellar spectrum, we assume a model form suggested by Padovani et al. (2018b),

$$j_p^{\mathrm{IS}}(E) = C\frac{E^{-a}}{(E+E_0)^b}\,\mathrm{cm}^{-2}\,\mathrm{s}^{-1}\,\mathrm{eV}^{-1}\,\mathrm{sr}^{-1}, \quad (16)$$

with $C = 2.4 \times 10^{15}$ and $E_0 = 650\,\mathrm{MeV}$. Two characteristic models are considered: a "high" (soft) spectrum $\mathscr{H}$ with $a = 0.8$ and a "low" (hard) spectrum $\mathscr{L}$ with $a = -0.1$, both having the same high-energy asymptote with $a + b = 2.7$. The spectrum $\mathscr{H}$ has been previously introduced to fit available data on H_2 ionization in diffuse clouds (Padovani et al. 2018b), while the spectrum $\mathscr{L}$ represents the proton spectrum measured down to $E = 3\,\mathrm{MeV}$ by the Voyager 1 spacecraft (Cummings et al. 2016) and extrapolated to the lower energies with the constant slope (Padovani et al. 2018b).

4. Balance Equation for the Electron Spectrum

Unlike protons, the continuous slowing-down approximation is not applicable for electrons. Below we show that the difference of the population and depopulation rates for secondary ionization (see Section 4.2) *cannot* be presented in a differential form, as the energy exchange in such collisions is not small, and the electron indistinguishability leaves a non-negligible integral term (see Appendix C).

At the same time, transport of secondary electrons is negligible. Indeed, Equation (B3) in Appendix B suggests that the local proton spectrum (determining primary ionization) varies at a column scale of $\sim N$ for $E \lesssim E_{\mathrm{att}}(N)$, and remains approximately constant for higher E. The fact that the ionization (and hence also excitation) loss functions of electrons and protons, $L_e(E_e)$ and $L_p(E_p)$, respectively, are

[3] Stopping ranges of different CR species are plotted in Figure 2 of Padovani et al. (2018b).

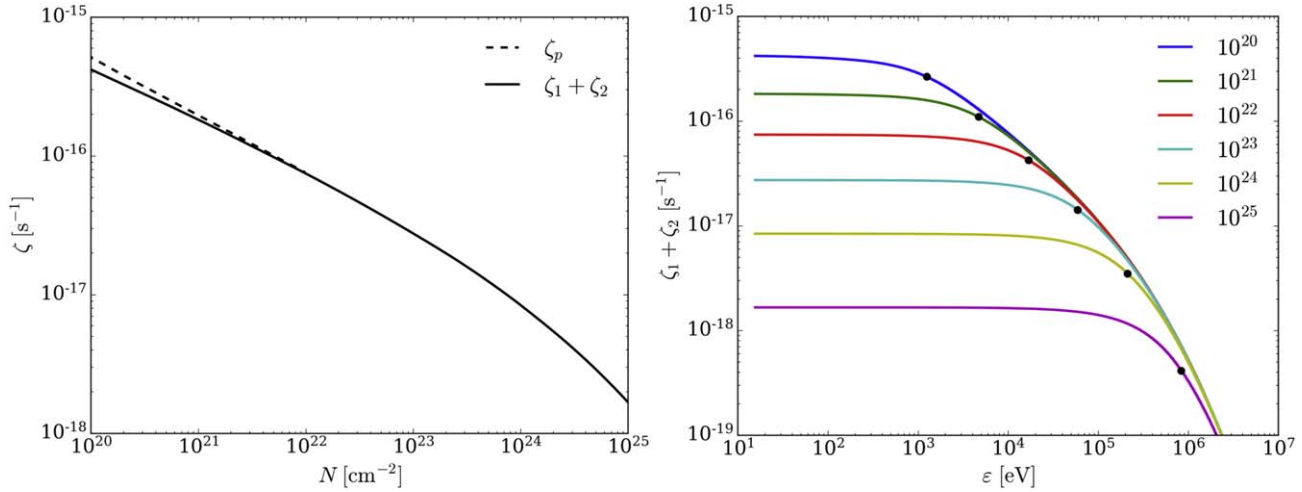

Figure 1. Left panel: rates of primary ionization of H_2 vs. the gas column density N, computed using the continuous slowing-down approximation (see Section 3) for the interstellar proton spectrum $\mathscr{H}$. The dashed line shows the dependence $\zeta_p(N)$ derived for the exact cross section of proton impact ionization (Rudd et al. 1992), the solid line represents the sum $\zeta_1+\zeta_2$ obtained from Equations (20) and (21) for $\varepsilon = I$. Right panel: $\zeta_1+\zeta_2$ vs. ε for different values of N (see the legend, in units of cm^{-2}). At smaller ε, each curve converges to the value shown by the solid line in the left panel. The bullets indicate where $\varepsilon = \varepsilon_{\rm att}(N)$.

comparable for equal particle velocities allows us to write the relation $L_e/L_p \sim (m_e/m_p)(E_p/E_e)$, valid with logarithmic accuracy for $E_e \gg I$ and $E_p \gg (m_p/m_e)I$. With the same accuracy, from Equation (13), we derive $L_e/L_p \sim (E_e/E_p)(R_p/R_e)$, and combining it with the preceding relation obtain $R_e/R_p \sim (m_p/m_e)(E_e/E_p)^2$. Since $E_e \lesssim 4(m_e/m_p)E_p$, substituting Equation (14) yields $R_e/N \sim 10 m_e/m_p \sim 0.01$ for the maximum stopping range of electrons produced at a given column density. Therefore, we can safely assume that secondary electrons are attenuated locally.

Thus, the steady-state spectrum $j_{\rm sec}(\varepsilon)$ is governed by the *local* balance of primary ionization and various loss mechanisms. Below we derive the balance equation for $j_{\rm sec}(\varepsilon)$, considering the secondary ionization and excitation as the major loss processes.

4.1. Primary Ionization

Consider the production of secondary electrons upon the proton impact ionization of the gas. The source term due to the primary ionization at a given column density N, viz., the number of electrons produced at energy ε (per unit time per gas particle) by CR protons with the local spectrum $j_p(E, N)$, is

$$\mathcal{P}_p(\varepsilon, N) = \int_{\frac{1}{4}\frac{m_p}{m_e}(\varepsilon+I)}^{\infty} \frac{\partial \sigma_p}{\partial \varepsilon}(E, \varepsilon) j_p(E, N)\, dE. \tag{17}$$

To take into account the fact that the attenuation of interstellar CRs generally creates anisotropy with respect to the magnetic field lines (see Section 3), the CR spectrum in Equation (17) is averaged over the pitch angles, i.e.,

$$j_p(E, N) = \frac{1}{2}\int_{-1}^{1} j_p(E, N, \mu)\, d\mu. \tag{18}$$

Assuming the integral over E to be dominated by proton energies much larger than $\frac{1}{4}(m_p/m_e)I \sim 10^4$ eV, we can substitute Equation (1) in Equation (17) and present the latter in the following form:

$$\mathcal{P}_p(\varepsilon, N) = \frac{1}{2\pi(1+\tilde{\varepsilon})^3 I}[\zeta_1(\varepsilon, N) + \tilde{\varepsilon}\zeta_2(\varepsilon, N)], \tag{19}$$

where the rates

$$\zeta_1(\varepsilon, N) = 2\pi\eta_p I \int_{\frac{1}{4}\frac{m_p}{m_e}(\varepsilon+I)}^{\infty} f_p(E) \ln\left(\frac{m_e}{m_p}\tilde{E}\right) \times j_p(E, N)\, dE, \tag{20}$$

$$\zeta_2(\varepsilon, N) = 2\pi I \int_{\frac{1}{4}\frac{m_p}{m_e}(\varepsilon+I)}^{\infty} f_p(E) j_p(E, N)\, dE, \tag{21}$$

are functionals of the local proton spectrum.[4] Thus, ζ_1 and ζ_2 determine the magnitude of the source term at low and high ε, respectively.

For the following analysis, it is convenient to introduce the electron energy scale $\varepsilon_{\rm att}$, related to the proton attenuation energy (15) via

$$\varepsilon_{\rm att}(N) = 4\frac{m_e}{m_p}E_{\rm att}(N) \approx 4.8\, N_{21}^{0.55}\ \text{keV}. \tag{22}$$

Taking into account Equation (6), the sum $\zeta_1+\zeta_2$ is the integral of the product $4\pi\sigma_{{\rm ion},p}(E) j_p(E, N)$. Hence, for small ε, it tends to the actual rate of the local primary ionization, $\zeta_p(N)$. Equation (B3) shows that $j_p(E, N)$ is peaked at $E \sim E_{\rm att}(N)$, and therefore, the sum remains independent of ε and equal to $\zeta_p(N)$ for $\varepsilon \ll \varepsilon_{\rm att}(N)$. The latter is demonstrated in the left panel of Figure 1, obtained for the interstellar proton spectrum $\mathscr{H}$: here, $\zeta_1+\zeta_2$ computed for $\varepsilon = I$ is plotted versus N along with the dependence $\zeta_p(N)$ derived from a precise expression for the ionization cross section (Rudd et al. 1992). The two curves nearly coincide for $N \gtrsim 10^{21}$ cm^{-2}, showing that the solid line is expected to accurately represent $\zeta_p(N)$ even for diffuse envelopes of molecular clouds. As expected—see discussion after Equation (1)—a noticeable deviation is only seen around $N \sim 10^{20}$ cm^{-2}, where $E_{\rm att}(N) \sim 10(m_p/m_e)I$ and hence the adopted $\sigma_{{\rm ion},p}(E)$ becomes slightly inaccurate.

For $\varepsilon \gtrsim \varepsilon_{\rm att}(N)$, both ζ_1 and ζ_2 become asymptotically independent of N. Given $f_p(E) \propto E^{-1}$, they fall off with ε approximately as $\zeta_1(\varepsilon) \propto j_p^{\rm IS}\left(\frac{1}{4}\frac{m_p}{m_e}\varepsilon\right)\ln\tilde{\varepsilon}$ and $\zeta_2(\varepsilon) \propto j_p^{\rm IS}\left(\frac{1}{4}\frac{m_p}{m_e}\varepsilon\right)$,

[4] For the assumed values of E, we can omit I in the lower integration limit.

as determined by the form of the interstellar spectrum. The right panel of Figure 1 illustrates this behavior for the interstellar spectrum $\mathscr{H}$. Here, $\zeta_1+\zeta_2$ is plotted versus ε for different values of N, showing how individual curves approach a common decreasing asymptote at $\varepsilon \gtrsim \varepsilon_{\rm att}(N)$ and tend to the plateau $\approx \zeta_p(N)$ at lower ε.

4.2. Secondary Ionization

The rate $\mathcal{P}_{\rm sec}(\varepsilon)$ at which secondary ionization collisions contribute to the population of electrons with energy ε (at given N) can be easily calculated using Equations (2)–(4). Setting the energy of a colliding electron to $E=\varepsilon+\varepsilon'+I$ and integrating the product $\partial\sigma_e/\partial\varepsilon(E,\,\varepsilon)\,j_{\rm sec}(E)$ over ε', we obtain

$$4\pi I\mathcal{P}_{\rm sec}(\varepsilon)=\int_0^\infty \varphi_{\rm M}(\varepsilon,\,\varepsilon')F(\varepsilon+\varepsilon'+I)\,d\varepsilon' + \eta_e\int_0^\infty \varphi_{\rm dip}(\varepsilon,\,\varepsilon')\ln(\tilde{\varepsilon}+\tilde{\varepsilon}'+1) \times F(\varepsilon+\varepsilon'+I)\,d\varepsilon'. \quad (23)$$

Here, to simplify the presentation of the results in the following text, we added the factor $4\pi I$ in order to introduce an auxiliary function F for the secondary spectrum (of dimensions $\mathrm{eV}^{-1}\,\mathrm{s}^{-1}$),

$$F(\varepsilon)\equiv 4\pi I f_e(\varepsilon) j_{\rm sec}(\varepsilon). \quad (24)$$

The rate of depopulation, $\mathcal{D}_{\rm sec}(\varepsilon)$, is simply equal to

$$\mathcal{D}_{\rm sec}(\varepsilon)=\sigma_{{\rm ion},e}(\varepsilon) j_{\rm sec}(\varepsilon). \quad (25)$$

4.3. Excitation

Consider electron collisions leading to excitation of state k of a molecule, characterized by the excitation energy Δ_k. The difference of the corresponding population and depopulation rates is

$$\mathcal{P}_{{\rm exc},k}(\varepsilon)-\mathcal{D}_{{\rm exc},k}(\varepsilon) = \sigma_{{\rm exc},k}(\varepsilon+\Delta_k) j_{\rm sec}(\varepsilon+\Delta_k)-\sigma_{{\rm exc},k}(\varepsilon) j_{\rm sec}(\varepsilon), \quad (26)$$

where $\sigma_{{\rm exc},k}(\varepsilon)$ is the excitation cross section of state k (see Dalgarno et al. 1999 and references therein).

4.4. Balance Equation

By summing up different contributions to the population and depopulation rates of electrons with energy ε, we obtain the following balance equation for the spectrum of secondary electrons:

$$\frac{2}{(1+\tilde{\varepsilon})^3}[\zeta_1(\varepsilon,N)+\tilde{\varepsilon}\zeta_2(\varepsilon,N)] +\int_0^\infty \varphi_{\rm M}(\varepsilon,\,\varepsilon')F(\varepsilon+\varepsilon'+I)\,d\varepsilon' +\eta_e\int_0^\infty \varphi_{\rm dip}(\varepsilon,\,\varepsilon')\ln(\tilde{\varepsilon}+\tilde{\varepsilon}'+1)F(\varepsilon+\varepsilon'+I)\,d\varepsilon' +I\sum_k \Phi_{{\rm exc},k}(\varepsilon+\Delta_k)F(\varepsilon+\Delta_k) =I\left[\Phi(\varepsilon)+\sum_k \Phi_{{\rm exc},k}(\varepsilon)\right]F(\varepsilon), \quad (27)$$

where dimensionless auxiliary functions for the ionization and excitation cross sections are

$$\Phi(\varepsilon)=\frac{\sigma_{{\rm ion},e}(\varepsilon)}{f_e(\varepsilon)I} \quad \text{and} \quad \Phi_{{\rm exc},k}(\varepsilon)=\frac{\sigma_{{\rm exc},k}(\varepsilon)}{f_e(\varepsilon)I},$$

respectively, and the dependence of F on N is not indicated for brevity.

Equation (27) assumes collisions with the most abundant gas species, i.e., with hydrogen molecules. Collisions with He and other gas species can be straightforwardly included by adding the corresponding terms (primary and secondary ionization plus excitation) multiplied by the species abundance. In principle, a contribution of interstellar CR electrons could also be included: this does not change the structure of Equation (27), since interstellar and secondary electrons are indistinguishable. On the other hand, it results in an additional advection term (analogous to the first term in Equation (12) for protons) and thus makes a solution of the balance equation much more complicated. However, according to Padovani et al. (2018b), the primary ionization is believed to be completely controlled by CR protons if their spectrum is close to the model form $\mathscr{H}$ (for the spectrum $\mathscr{L}$, it is true for $N\gtrsim 10^{22}\,\mathrm{cm}^{-2}$), and therefore, we neglect the effect of interstellar electrons in this paper.

Finally, we note that Equation (27) can be easily generalized to compute the secondary electron spectrum produced by X-rays. In this case, j_p and $\partial\sigma_p/\partial\varepsilon$ in the source term due to proton ionization, Equation (17), are replaced by the corresponding X-ray spectrum and differential cross section, while the lower limit of integration over the X-ray energy is $\varepsilon+I$. This only leads to a different functional form of the first term in Equation (27).

4.5. Effect of Coulomb Collisions

The Coulomb collisions with free electrons could be included in Equation (27), too, by adding the corresponding rates multiplied by the gas ionization fraction $n_e/n_{\rm gas}$. The population rate is given by the first integral in Equation (23) with $I=0$ and $\varphi_{\rm M}(\varepsilon,\,\varepsilon')$ described by classical Mott's formula for free electrons (Landau & Lifshitz 1991), i.e., by Equation (3) without unity in the denominators; the depopulation rate is proportional to the integral over this $\varphi_{\rm M}(\varepsilon,\,\varepsilon')$.

Obviously, the resulting integrals contain terms diverging as $\propto 1/\varepsilon'$ at $\varepsilon'\to 0$. This artificial divergence is avoided in the balance equation by writing the difference of the population and depopulation rates as $I^2\ln(\varepsilon/\varepsilon_{\rm min})F'(\varepsilon)$ plus non-diverging terms; here $F'(\varepsilon)$ denotes a derivative over ε, and the factor I^2 comes from the common energy normalization. The minimum truncation energy $\varepsilon_{\rm min}\sim(\delta p_{\rm min})^2/2m_e$ is determined by the minimum momentum $\delta p_{\rm min}\sim e^2/(b_{\rm max}v)$ that can be transferred by a secondary electron (with the velocity $v=\sqrt{2\varepsilon/m_e}$) to the surrounding free electrons (whose plasma frequency is $\omega_{pe}=\sqrt{4\pi e^2 n_e/m_e}$) at the maximum impact parameter $b_{\rm max}\sim v/\omega_{pe}$. The resulting logarithmic factor $\ln(\varepsilon/\varepsilon_{\rm min})\sim 3\ln(\varepsilon/e^2 n_e^{1/3})$ is estimated to be $\lesssim 90$ for nonrelativistic electrons. Hence, for the gas ionization fractions of $\lesssim 10^{-4}$, typical for molecular clouds, the contribution of Coulomb collisions should be completely negligible.

5. Spectrum of Secondary Electrons

In this section we analyze generic properties of the secondary electron spectra $j_{\rm sec}(\varepsilon, N)$, related via Equation (24) to the solution of balance Equation (27). We consider only excitation of electronic states; rotational and vibrational excitation, occurring at $\varepsilon < I$, are neglected. First, we derive the analytical asymptotes valid for sufficiently high electron energies, and then compare this with exact numerical solution, which allows us to elucidate the role of different inelastic processes in shaping the electron spectrum.

5.1. Analytical Solution at High Energies

To evaluate the high-energy solution of Equation (27), describing the electron spectrum at $\varepsilon \gg I$, let us first neglect excitation collisions. As shown in Section 5.2, their addition does not qualitatively affect the results at high energies.

The right panel of Figure 1 demonstrates that the rates ζ_1 and ζ_2 are practically independent of ε for $\varepsilon \ll \varepsilon_{\rm att}(N)$, so that their sum is $\approx \zeta_p(N)$. On the other hand, for the interstellar spectrum $\mathscr{H}$, both terms start rapidly decreasing at $\varepsilon \gtrsim \varepsilon_{\rm att}$. Thus, for the analytical solution in this case, it is reasonable to approximate both ζ_1 and ζ_2 by step-functions, set to the respective (N-dependent) constants at $\varepsilon \lesssim \varepsilon_{\rm att}$ and to zero at larger ε. We note that the step-function approximation becomes exact for a monoenergetic local spectrum of protons with $E = E_{\rm att}(N)$.

For $\tilde{\varepsilon}$ much larger than $\eta_p \ln\tilde{\varepsilon}_{\rm att}$, the primary ionization in Equation (27) is dominated by the term $\propto \zeta_2$. In Appendix C we derive the following leading energy dependence for $\eta_p \ln\tilde{\varepsilon}_{\rm att} \ll \tilde{\varepsilon} \ll \tilde{\varepsilon}_{\rm att}$:

$$F(\varepsilon, N) \approx \frac{2\zeta_2(N)}{(1+\eta_e)I}\,\frac{(\ln\tilde{\varepsilon}_{\rm att})^{\frac{1}{1+\eta_e}}}{\tilde{\varepsilon}\,(\ln\tilde{\varepsilon})^{1+\frac{1}{1+\eta_e}}}, \tag{28}$$

where the dependence on N is given by Equation (21) evaluated at $\varepsilon = I$. In Appendix C we also obtain a rough estimate for the solution at lower energies, where the primary ionization is dominated by the term $\propto\zeta_1$. Assuming $1 \ll \tilde{\varepsilon} \ll \eta_p \ln\tilde{\varepsilon}_{\rm att}$ yields

$$F(\varepsilon, N) \sim \frac{\zeta_1(N)}{(1+\eta_e)I}\,\frac{1}{\tilde{\varepsilon}^2}, \tag{29}$$

with $\zeta_1(N)$ from Equation (20). This estimate neglects a factor $\sim$1, which logarithmically depends on ε.

We remind the reader that the physical spectrum of secondary electrons at $\tilde{\varepsilon} \gg 1$ scales as $j_{\rm sec}(\varepsilon) \propto \varepsilon F(\varepsilon)$, as follows from Equation (24). Therefore, the spectrum is characterized by a long tail decreasing logarithmically with energy up to $\varepsilon \sim \varepsilon_{\rm att}(N)$. In particular, this implies that the average energy of secondary electrons $\langle\varepsilon_{\rm sec}\rangle$ increases with N; using Equation (28), we readily obtain the following dependence:

$$\langle\varepsilon_{\rm sec}\rangle \approx \frac{1}{3}\varepsilon_{\rm att}(N), \tag{30}$$

derived assuming $\ln\tilde{\varepsilon}_{\rm att} \gg 1$. It is important to stress that $\langle\varepsilon_{\rm sec}\rangle$ is much larger than the average energy of electrons ejected in ionizing (primary or secondary) collisions, which is generally calculated as $\langle\varepsilon_{\rm ej}\rangle = L(E)/\sigma_{\rm ion}(E) - I$. The latter is sometimes erroneously employed in literature to characterize the average energy of secondary electrons. For primary ionization, assuming proton energies $E \gg (m_p/m_e)I$, we can use Equation (1) for $\partial\sigma_p/\partial\varepsilon$. Substituting this into Equation (A5), we derive the leading logarithmic term for the proton loss function, $L_p(E) \approx f_p(E)I^2(1+\eta_p)\ln(\frac{m_e}{m_p}\tilde{E})$. With the logarithmic term in the ionization cross section $\sigma_{{\rm ion},p}(E)$ from Equation (6), we obtain that the average energy of electrons ejected by high-energy protons tends to $\langle\varepsilon_{{\rm ej},p}\rangle \to (1+2/\eta_p)I$; the same line of arguments yields $\langle\varepsilon_{{\rm ej},e}\rangle \to (1+2/\eta_e)I$ for the secondary ionization. Thus, the average energy of ejected electrons at large N tends to a constant value of $\langle\varepsilon_{\rm ej}\rangle \sim 3I$ (since $\eta_{p,e} \sim 1$), while the average energy of the actual secondary spectrum follows Equation (30).

Equations (28) and (29) can be extended to a case where excitation collisions are taken into account. For large ε, the cross sections for the electron-impact excitation of H_2 singlet states behave similar to the ionization cross section (see, e.g., Dalgarno et al. 1999; Janev et al. 2003), i.e., their ratios tend to constant values. As shown in Appendix C, the solution in this case is still given by Equation (28) with η_e replaced by

$$\eta_e^* = \left[1 + \frac{1}{2}\sum_k \frac{\Delta_k}{I}\left(\frac{\sigma_{{\rm exc},k}}{\sigma_{{\rm ion},e}}\right)_\infty\right]\eta_e, \tag{31}$$

where the cross-sectional ratios are evaluated at $\varepsilon \to \infty$.

5.2. Numerical Solution and Its Analysis

The excitation cross sections of H_2 singlet and triplet states were taken from Janev et al. (2003). The function $f_e(E)$, relating F and $j_{\rm sec}$ in Equation (24), was derived from Equation (3) in Kim et al. (2000). Equation (27) was solved numerically for discrete values of columns between $N = 10^{20}\,{\rm cm}^{-2}$ and $N = 10^{25}\,{\rm cm}^{-2}$, by implementing an iterative procedure for $F(\varepsilon)$ (similar to the solution of Volterra-type integral equations). The next-iteration function $F_{i+1}(\varepsilon)$ was obtained by evaluating the lhs of Equation (27) for $F_i(\varepsilon)$, and then using this result to solve for $F_{i+1}(\varepsilon)$ on the rhs. This procedure was repeated until $|F_{i+1} - F_i| \leqslant 10^{-6}F_i$ at any ε. The convergence at smaller columns was relatively fast and rather insensitive to the initial trial $F_0(\varepsilon)$. To facilitate the convergence at larger columns, the initial trial for the next value of N was the solution for the previous N.

Figure 2 displays $j_{\rm sec}(\varepsilon, N)$ computed for the interstellar proton spectrum $\mathscr{H}$. The model case of no excitation is depicted in the left panel ("no exc") by curves for different values of N. These curves are well described by the high-energy analytical solution (28), as illustrated in the inset for $N = 10^{25}\,{\rm cm}^{-2}$. To facilitate the comparison with analytical results, we replaced the assumed step-function energy dependence of ζ_2 in Equation (28) by the actual form determined by Equation (21) for the spectrum $\mathscr{H}$. We see that the analytical curve in the inset remains accurate to within 30% for $\varepsilon \gtrsim I\ln\tilde{\varepsilon}_{\rm att}$ ($\sim 10^2$ eV) and $\varepsilon \ll \varepsilon_{\rm att}$ ($\sim 10^6$ eV). Remarkably, the agreement remains reasonable (within a factor of two to three) also for energies outside the assumed range of applicability.

Inclusion of excitation does not qualitatively change the form of $j_{\rm sec}(\varepsilon)$ except for energies in the vicinity of the ionization potential, as is evident from the right panel ("exc") of Figure 2. The inset shows that excitation reduces $j_{\rm sec}(\varepsilon)$ by $\lesssim$20% at $\varepsilon \gtrsim 1$ keV, almost irrespective of N; the reduction is stronger at smaller ε, and the dependence on N becomes more

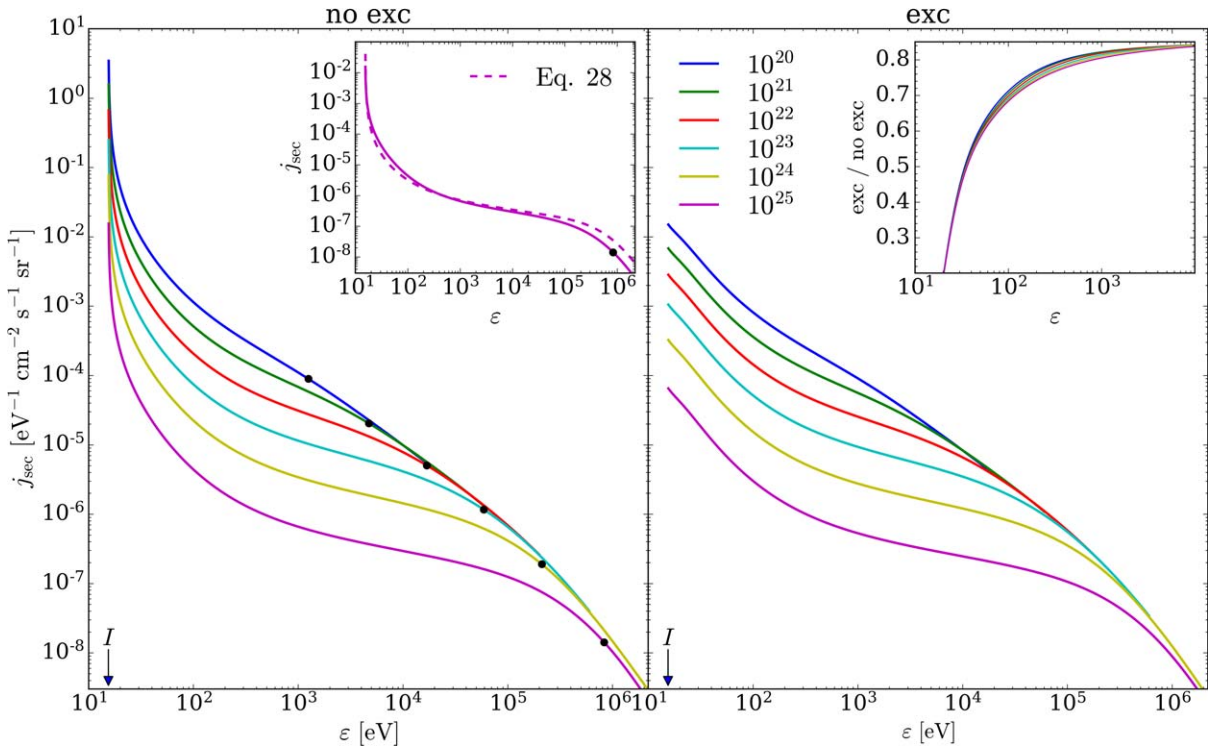

Figure 2. Energy spectra of secondary electrons $j_{sec}(\varepsilon)$ obtained for the interstellar proton spectrum $\mathscr{H}$ from a numerical solution of Equation (27) for different N (see the legend, in units of cm^{-2}). The vertical arrows in the bottom left corners of the panels indicate where $\varepsilon = I$. The left panel shows the spectra for a model case where excitation collisions are omitted; agreement between the numerically computed spectrum and the high-energy analytical asymptote, Equation (28), is illustrated for $N = 10^{25}$ cm^{-2} in the inset. The bullets for different curves indicate where $\varepsilon = \varepsilon_{att}(N)$. The right panel displays the results with excitation; the inset shows these spectra normalized by $j_{sec}(\varepsilon)$ that are plotted in the left panel.

pronounced. This trend is described by the excitation correction of Equation (31), leading to a reduction of high-energy spectra (28). Excitations of H_2 singlet and triplet states contribute differently to this effect: cross sections $\sigma_{exc,k}(\varepsilon)$ for triplet states have a peak localized between 10–20 eV and rapidly decrease at larger ε, whereas for singlet states, they have a broader peak between ~30–100 eV, overlapping with the peak of $\sigma_{ion,e}(\varepsilon)$, and behave similarly to $\sigma_{ion,e}(\varepsilon)$ also at large ε. As discussed in the next section, singlet excitations almost completely determine the magnitude of the secondary ionization rate, while the role of triplet excitations is minor.

We note that the strong deviation seen between the left and right panels near the ionization potential originates from the simple fact that, without excitation, the product $\sigma_{ion,e}(\varepsilon) j_{sec}(\varepsilon)$ on the rhs of Equation (27) remains finite as $\varepsilon \to I$, thus leading to artificial divergence $j_{sec}(\varepsilon) \propto (\varepsilon - I)^{-1}$ in this case. This divergence does not significantly affect the calculation of ζ_{sec}, because electrons with $\varepsilon \approx I$ provide a minor contribution to its value.

6. Secondary Ionization Rate

The rate of local secondary ionization can be conveniently rewritten in terms of the auxiliary functions Φ and F,

$$\zeta_{sec}(N) = \int_I^\infty \Phi(\varepsilon) F(\varepsilon, N)\, d\varepsilon. \quad (32)$$

To obtain the ratio ζ_{sec}/ζ_p versus N, we derive $\zeta_{sec}(N)$ by substituting the numerical solution of Equation (27), and calculate $\zeta_p(N)$ as explained in Section 4.1. For methodological reasons, here we also discuss the model case of no excitation collisions—this helps us to explore their impact on ζ_{sec} and to reveal the role of the interstellar proton spectrum. To characterize the effect of qualitatively different proton spectra, here we present the results for both spectra $\mathscr{H}$ and $\mathscr{L}$.

Figure 3 summarizes our findings for ζ_{sec}/ζ_p. We see that this ratio steadily increases with column density: the trend is almost unaltered between the curves computed with and without excitation, and is present for both proton spectra (though it is substantially weaker for the spectrum $\mathscr{L}$, see discussion below). In Appendix D it is shown that ζ_{sec}/ζ_p keeps increasing at any physically relevant value of N. This behavior is quite different form the traditional assumption of a constant ζ_{sec}/ζ_p with the "canonical" value of ≈0.67 (e.g., Spitzer & Tomasko 1968).

We begin with the analysis of the results for the spectrum $\mathscr{H}$, shown by the *thick solid lines* in Figure 3. The red line depicts ζ_{sec}/ζ_p versus N for the "exc" case, where excitation collisions are included. We see that this curve is shifted substantially down with respect to the model "no exc" case (depicted by the black line), and that the slope of the "exc" curve is slightly smaller at larger N. This behavior follows from the inset in the right panel of Figure 2: excitation causes a reduction of $j_{sec}(\varepsilon)$ by 30%–60% at energies between ~30–100 eV, corresponding to the maximum of the ionization cross section (hence leading to an efficient decrease of ζ_{sec}), and the reduction is slightly stronger for larger N. As noted in Section 5.2, H_2 excitation is completely dominated by singlet states for $\varepsilon \gtrsim 30$ eV, and therefore the effect of triplet states on ζ_{sec}/ζ_p is minor: the "exc" curve computed for singlet excitation only would be shifted up by less than 10% with

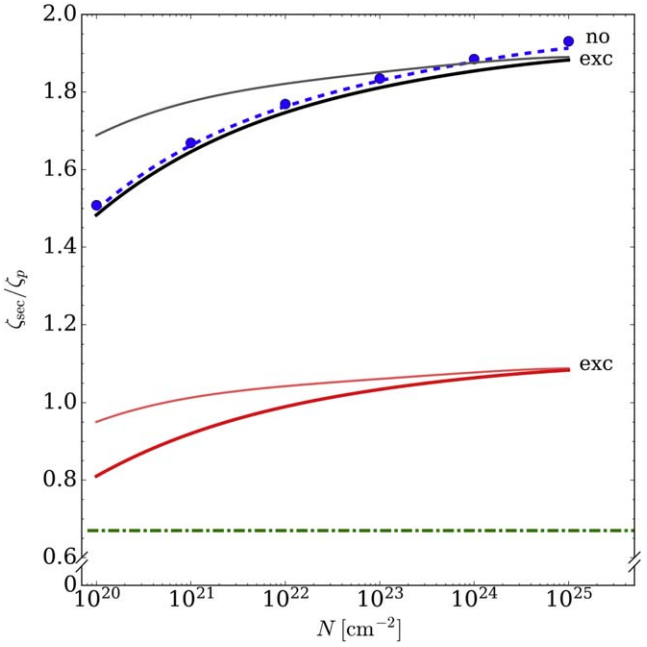

Figure 3. Ratio of the secondary to primary ionization rates of H_2, ζ_{sec}/ζ_p, as a function of the gas column density, N, computed using the continuous slowing-down approximation for protons (Section 3) and a numerical solution of Equation (27) for secondary electrons. Pairs of the thicker and thinner solid lines represent results for the interstellar proton spectrum $\mathscr{H}$ and $\mathscr{L}$, respectively. The pair of red curves ("exc") shows the case where excitation collisions with H_2 are included. For methodological reasons, we also plot the model case of no excitation ("no exc"). Here, in addition to the pair of black curves, the approximation of monoenergetic local protons with $E = E_{att}(N)$ is also depicted: the dashed line represents the numerical solution of Equation (27), and the bullets show the results of Monte Carlo simulations. For comparison, the horizontal dashed–dotted line indicates the value of $\zeta_{sec}/\zeta_p \approx 0.67$ commonly adopted in the literature.

respect to the curve shown in Figure 3. Also, the results are virtually independent of the (poorly constrained) value of the prefactor η_e in Equation (2), varying by less than 1% for $0.6 \leqslant \eta_e \leqslant 1$.

Let us now discuss the role of the proton spectrum (considering for simplicity the "no exc" case). For sufficiently soft interstellar spectra, such as $\mathscr{H}$, the resulting local spectrum $j_p(E, N)$ is peaked at $E \sim E_{att}(N)$, as follows from Equation (B3). In Section 5.1 we pointed out that this fact allows us to approximate the rates of primary ionization $\zeta_{1,2}(\varepsilon, N)$ by step-functions of ε, which is equivalent to the approximation of monoenergetic local protons with $E = E_{att}(N)$. The dashed line in Figure 3 shows ζ_{sec}/ζ_p versus N computed for this approximation, demonstrating a remarkably good agreement with the corresponding thick solid line. To ensure an accurate comparison, $E_{att}(N)$ was derived from the exact stopping range of protons, as presented in Padovani et al. (2018b).

Thus, the dependence of ζ_{sec}/ζ_p on N computed for the model spectrum $\mathscr{H}$ must be representative of any sufficiently soft spectrum of interstellar protons. On the other hand, for extremely hard model spectra—such as $\mathscr{L}$, increasing at nonrelativistic energies—a monoenergetic approximation of local protons is no longer justified. In this case, unattenuated protons with $E_{att}(N) \lesssim E \lesssim E_0$ provide a significant contribution to primary ionization. The *thin solid lines* in Figure 3 show ζ_{sec}/ζ_p calculated for the spectrum $\mathscr{L}$, demonstrating that the resulting dependence on N is noticeably weaker than that for $\mathscr{H}$.

Available observational data on the H_2 ionization in a large number of diffuse clouds (Indriolo & McCall 2012; Neufeld & Wolfire 2017) tend to favor soft interstellar spectra. Assuming the continuous slowing-down approximation for CR protons, the spectrum $\mathscr{H}$ provides a reasonable approximation of the data, while the spectrum $\mathscr{L}$ (which represents the Voyager measurements, probing the very local ISM within the Local Bubble) underestimates the ionization rate in diffuse clouds by more than an order of magnitude (Padovani et al. 2018b). Moreover, the spectrum $\mathscr{L}$ fails to recover the suggested dependence on N. Therefore, based on our current knowledge, one should consider the above results obtained for the spectrum $\mathscr{H}$ as representative.

The fact that the approximation of monoenergetic local protons accurately describes the secondary ionization for soft interstellar spectra allows us to substantiate and complement the above calculations by Monte Carlo simulations. In Appendix E we describe a simple algorithm to compute ζ_{sec}/ζ_p for monoenergetic protons directly, based on the differential ionization cross sections given by Equations (1) and (2). Results of the direct simulations are depicted in Figure 3 by the bullets, showing excellent agreement with the dashed line.

Finally, adding interstellar CR nuclei heavier than protons does not significantly change the calculated values of ζ_{sec}/ζ_p. To estimate this effect, we keep in mind that the differential cross section of impact ionization by a nucleus with the atomic number Z is proportional to Z^2 and is determined by the nucleus velocity (Landau & Lifshitz 1991). Assuming that Equation (1) describes the functional form of the differential cross section for any nucleus, from Equation (13), it follows that the attenuation energy per nucleon is equal to $E_{att}(Z^2N/A)$, where A is the nucleus mass number. Hence, substituting $N \to Z^2N/A$ in a function describing the dependence ζ_{sec}/ζ_p versus N for protons, we obtain the corresponding dependence for nuclei. We employ this fact in Appendix F to show that the expected effect of heavier CR nuclei is to increase the ratios plotted in Figure 3 by less than 1%.

7. Conclusion and Implications

Our aim was to rigorously calculate the energy spectrum of secondary electrons that are produced by interstellar CRs penetrating into dense regions of the ISM. The results are completely determined by the differential cross sections of the proton impact (primary) and electron-impact (secondary) ionization as well as by the electron excitation cross sections of the gas species. We derived the governing balance equation that yields the secondary electron spectrum as a function of the gas column density for a given regime of the proton penetration into dense gas; in this paper, the commonly used free-streaming regime was assumed.

The principal findings can be summarized as follows:

1. The secondary electron spectrum $j_{sec}(\varepsilon, N)$ has a long tail decreasing logarithmically with the energy ε, as described by the universal analytical asymptote (28) for the auxiliary spectrum function $F(\varepsilon) \propto j_{sec}(\varepsilon)/\varepsilon$. The effect

of excitation collisions at high energies is generally described by Equation (31).

2. The characteristic maximum energy of the secondary spectrum, $\varepsilon_{\rm att}(N)$, increases with the gas column N according to Equation (22). The maximum energy is proportional to the proton attenuation energy $E_{\rm att}(N)$, and the average energy of the secondary electrons is $\sim\frac{1}{3}\varepsilon_{\rm att}(N)$.
3. The ratio of the secondary to primary ionization rates, $\zeta_{\rm sec}/\zeta_p$, is a monotonically increasing function of the gas column for any relevant value of N. The value of $\zeta_{\rm sec}/\zeta_p$ varies between ≈ 0.8 and ≈ 1.1 for $10^{20}\,{\rm cm}^{-2} \leqslant N \leqslant 10^{25}\ {\rm cm}^{-2}$, as depicted by the thick red line in Figure 3, and thus is substantially larger than the commonly adopted constant value of ≈ 0.67.
4. The derived dependence $\zeta_{\rm sec}/\zeta_p$ versus N is practically independent of a particular shape of the interstellar spectrum of protons (unless they have an extremely hard spectrum, such as the spectrum $\mathscr{L}$). This dependence can be accurately reproduced by using a monoenergetic local spectrum of protons with $E = E_{\rm att}(N)$.

Knowing the actual form of the secondary electron spectrum opens up the possibility of accurately reevaluating characteristics of several important processes driven by CRs in dark molecular clouds. The most notable and obvious examples include the gas heating, production of atomic hydrogen, and generation of UV photons. It is certainly beyond the scope of this paper to thoroughly analyze such processes, but we expect their characteristics to be significantly affected if the presented results are taken into account, as outlined below:

Gas heating. Secondary electrons should contribute to the gas heating through additional ionization and excitation channels. We can assess a relative energy budget for this process by comparing the rate of energy deposition due to secondary ionization/excitation with that due to primary ionization/excitation (but keeping in mind that only a fraction of the energy deposited by CRs is eventually converted into heat; see Glassgold et al. 2012 for detailed analysis). Defining the deposition rate $\dot{\mathcal{E}}$ as the loss function averaged over the secondary and primary spectrum, the ratio $\dot{\mathcal{E}}_{\rm sec}/\dot{\mathcal{E}}_p$ can be evaluated for large N by virtue of Equation (28), similar to how we did it in Appendix D for $\zeta_{\rm sec}/\zeta_p$. This yields the asymptotic ratio $\dot{\mathcal{E}}_{\rm sec}/\dot{\mathcal{E}}_p \to \frac{1}{2}(1 + 1/\eta_e)$, suggesting that the actual ratio of the heating rates (i) may not be equal to $\zeta_{\rm sec}/\zeta_p$, as universally assumed in modeling, and (ii) may be sensitive to the poorly constrained value of η_e.

Production of atomic hydrogen. Interstellar UV photons cannot penetrate the interiors of molecular clouds due to absorption by dust as well as H_2 line absorption, and therefore the destruction of molecular hydrogen in these regions is controlled by CRs. This process primarily occurs through electron-impact excitation of H_2 triplet states (Padovani et al. 2018a), whose cross sections peak between 10–20 eV and rapidly decrease at higher energies. For this reason, the rate of H_2 dissociation $\zeta_{\rm diss}$ must be particularly sensitive to the shape of the secondary electron spectrum near the ionization potential. The secondary spectrum used to compute H_2 dissociation in Padovani et al. (2018a) was derived from the continuous slowing-down approximation for electrons, leading to a practically constant ratio of $\zeta_{\rm diss}/(\zeta_p + \zeta_{\rm sec})$ at columns of $N \gtrsim 10^{21}\ {\rm cm}^{-2}$. Based on the results derived here for $\zeta_{\rm sec}/\zeta_p$, we expect the ratio for H_2 dissociation to vary with N, too.

Generation of UV photons. Excitation of H_2 singlet states by CRs produces fluorescence in the Lyman and Werner bands, leading to an efficient generation of UV fields in dark clouds (Prasad & Tarafdar 1983). The cross section of electron-impact excitation of singlet states behaves similarly to the ionization cross section at energies above ~30 eV, and therefore the shape of the entire spectrum of secondary electrons is important for this process. Available estimates of the UV field (Cecchi-Pestellini & Aiello 1992) are also based on the continuous slowing-down approximation for electrons, assuming the "canonical" value of $\zeta_{\rm sec}/\zeta_p \approx 0.67$, and therefore one may expect significant corrections for the UV field, too.

All three processes discussed above play an essential role in the physical and chemical evolution of molecular clouds, with profound implications for the formation of stars and circumstellar disks.

We would like to thank Paola Caselli and Valerio Lattanzi for useful discussions and suggestions. The work is supported by the Russian Science Foundation via Project 20-12-00047.

Appendix A
Differential Form of Energy Losses for Protons

Using Equation (5), we obtain the upper integration limit $\varepsilon^*_{{\rm max},p}(E)$ in Equation (10),

$$\varepsilon^*_{{\rm max},p} = \frac{\chi}{1-\chi}E - I, \tag{A1}$$

where $\chi \equiv 4(m_e/m_p)$ is a small parameter characterizing the fraction of energy transferred to electrons. This allows us to Taylor expand the integrand of Equation (10) over small $\varepsilon + I$. Keeping the first two terms yields

$$\mathcal{P}(E) \approx j_p(E)\int_0^{\varepsilon^*_{{\rm max},p}} \frac{\partial\sigma_p}{\partial\varepsilon}(E,\varepsilon)d\varepsilon + \int_0^{\varepsilon^*_{{\rm max},p}} \frac{\partial}{\partial E}\left[\frac{\partial\sigma_p}{\partial\varepsilon}(E,\varepsilon)j_p(E)\right](\varepsilon + I)\,d\varepsilon. \tag{A2}$$

From Equation (A1) we derive

$$\varepsilon^*_{{\rm max},p} - \varepsilon_{{\rm max},p} = \frac{\chi}{1-\chi}(\varepsilon_{{\rm max},p} + I),$$

where $\varepsilon_{{\rm max},p}$ is given by Equation (5). Hence, the difference $\mathcal{P} - \mathcal{D}$ in Equation (9) can be written with accuracy $O(\chi)$ as a sum of

$$\chi(\varepsilon_{{\rm max},p} + I)\frac{\partial\sigma_p}{\partial\varepsilon}(E,\varepsilon_{{\rm max},p})j_p(E), \tag{A3}$$

and the second term in Equation (A2). Since $\partial\varepsilon^*_{{\rm max},p}/\partial E \approx \chi$, this second term can be written as a derivative over E of the integral minus χ times the integrand taken at $\varepsilon = \varepsilon^*_{{\rm max},p}$. To the same accuracy, the latter cancels out with term (A3), and we

obtain

$$\mathcal{P} - \mathcal{D} = \frac{\partial}{\partial E}(L_p j_p) + O(\chi), \tag{A4}$$

where

$$L_p(E) = \int_0^{\varepsilon_{\max,p}(E)} (\varepsilon + I)\frac{\partial \sigma_p}{\partial \varepsilon}(E, \varepsilon)\, d\varepsilon, \tag{A5}$$

is the ionization loss function of protons.

Appendix B
Analytical Solution of Equation (12)

An explicit solution of Equation (12) can be derived for a power-law interstellar spectrum,

$$j_p^{\rm IS}(E) = j_0\left(\frac{E}{E_0}\right)^{-a}. \tag{B1}$$

Assuming CRs enter a cloud from one side ($\mu > 0$), and substituting a power-law approximation of the proton loss function (Padovani et al. 2018b; Silsbee & Ivlev 2019),

$$L_p(E) = L_0\left(\frac{E}{E_0}\right)^{-d}, \tag{B2}$$

valid for 4×10^5 eV $\lesssim E \lesssim 10^8$ eV (with $d = 0.81$ and $L_0 = 1.21\times 10^{-17}$ eV cm^2 for $E_0 = 650$ MeV), we obtain the following solution (see Appendix E of Padovani et al. 2018b):

$$j_p(E, N, \mu) = j_p^{\rm IS}(E)\left[1 + \frac{N}{\mu R_p(E)}\right]^{-\frac{a+d}{1+d}}, \tag{B3}$$

where

$$R_p(E) = \frac{E_0}{(1+d)L_0}\left(\frac{E}{E_0}\right)^{1+d}, \tag{B4}$$

is the proton stopping range for the loss function (B2).

Appendix C
High-energy Spectrum of Secondary Electrons

Let us first omit excitation collisions. In order to evaluate the high-energy spectrum at $\varepsilon \gg I$, we break the integrals on the lhs of Equation (27) into two parts: from 0 to ε ("integrals I"), and from ε to ∞ ("integrals II"). Since $\zeta_{1,2}$ rapidly decrease at $\varepsilon \gtrsim \varepsilon_{\rm att}$, we assume that $F(\varepsilon)$ vanishes at these energies. Below it is shown that the leading term of the high-energy spectrum depends logarithmically on $\varepsilon_{\rm att}$, and therefore we can truncate integrals II at $\varepsilon' = \varepsilon_{\rm att}$.

We substitute $\varphi_{\rm M}(\varepsilon, \varepsilon')$ and $\varphi_{\rm dip}(\varepsilon, \varepsilon')$ from Equations (3) and (4) into the integrals and neglect unity in the terms containing $1 + \tilde{\varepsilon}$. Then we *multiply* Equation (27) by $\tilde{\varepsilon}^2$ and write the resulting sum of integrals II in the following form:

$$\sum\int_{\varepsilon}^{\varepsilon_{\rm att}} \ldots \approx \int_{2\varepsilon}^{\varepsilon_{\rm att}} F(\varepsilon')\left\{1 - \frac{\varepsilon}{\varepsilon' - \varepsilon} + \left(\frac{\varepsilon}{\varepsilon' - \varepsilon}\right)^2 + \eta_e\frac{\ln\tilde{\varepsilon}'}{\tilde{\varepsilon}}\left[1 + \left(\frac{\varepsilon}{\varepsilon' - \varepsilon}\right)^3\right]\right\} d\varepsilon'. \tag{C1}$$

We see that the small terms $\propto \ln\tilde{\varepsilon}'/\tilde{\varepsilon}$ can be safely neglected. For the sum of integrals I, we obtain

$$\begin{aligned}\sum\int_0^{\varepsilon} \ldots \approx &\int_0^{\varepsilon} F(\varepsilon + \varepsilon' + I)\, d\varepsilon' \\ &- \tilde{\varepsilon}\int_0^{\varepsilon} \frac{F(\varepsilon + \varepsilon' + I)}{1 + \tilde{\varepsilon}'}\, d\varepsilon' \\ &+ \tilde{\varepsilon}^2\int_0^{\varepsilon} \frac{F(\varepsilon + \varepsilon' + I)}{(1 + \tilde{\varepsilon}')^2}\, d\varepsilon' \\ &+ \frac{\eta_e}{\tilde{\varepsilon}}\int_0^{\varepsilon} \ln(\tilde{\varepsilon} + \tilde{\varepsilon}' + 1) \\ &\times F(\varepsilon + \varepsilon' + I)\, d\varepsilon' \\ &+ \eta_e\tilde{\varepsilon}^2\int_0^{\varepsilon} \frac{\ln(\tilde{\varepsilon} + \tilde{\varepsilon}' + 1)}{(1 + \tilde{\varepsilon}')^3} \\ &\times F(\varepsilon + \varepsilon' + I)\, d\varepsilon'.\end{aligned} \tag{C2}$$

We Taylor expand $F(\varepsilon + \varepsilon' + I)$ and $\ln(\tilde{\varepsilon} + \tilde{\varepsilon}' + 1)$ over $\tilde{\varepsilon}' + 1$. Terms $\propto F(\varepsilon)$ include those leading in ε (from the second, third, and fifth integrals I), which exactly cancel out with the rhs terms. Keeping the remaining leading terms resulting from the expansion yields

$$\frac{1}{I}\sum\int_0^{\varepsilon} \ldots \approx (1 + \eta_e)\tilde{\varepsilon}\, F(\tilde{\varepsilon}) + (1 + \eta_e)\tilde{\varepsilon}^2 \ln\tilde{\varepsilon}\, F'(\tilde{\varepsilon}) + \frac{5}{12}\tilde{\varepsilon}^3\, F''(\tilde{\varepsilon}) + \ldots, \tag{C3}$$

where $F'(\tilde{\varepsilon})$ denotes the derivative with respect to $\tilde{\varepsilon}$. A posteriori analysis renders terms with the second and higher derivatives in Equation (C3) unimportant for the leading term of the sought solution.

For $\tilde{\varepsilon} \gg \eta_p \ln\tilde{\varepsilon}_{\rm att}$, the leading term due to primary ionization is $2\zeta_2$ (in the multiplied Equation (27)). Summing up, for $\eta_p \ln\tilde{\varepsilon}_{\rm att} \ll \tilde{\varepsilon} \ll \tilde{\varepsilon}_{\rm att}$, Equation (27) is reduced to

$$(1 + \eta_e)[\tilde{\varepsilon}^2 \ln\tilde{\varepsilon}\, \tilde{F}'(\tilde{\varepsilon}) + \tilde{\varepsilon}\, \tilde{F}(\tilde{\varepsilon})] + \int_{2\tilde{\varepsilon}}^{\tilde{\varepsilon}_{\rm att}} \tilde{F}(\tilde{\varepsilon}') \times \left[1 - \frac{1}{\tilde{\varepsilon}'/\tilde{\varepsilon} - 1} + \frac{1}{(\tilde{\varepsilon}'/\tilde{\varepsilon} - 1)^2}\right] d\tilde{\varepsilon}' + 1 = 0, \tag{C4}$$

where $\tilde{F} = (I/2\zeta_2)F$. We introduce a new variable $x = \ln\tilde{\varepsilon}$ and seek the solution of the form $\tilde{F}(\tilde{\varepsilon}) = ce^{-x}/x^{1+s}$. As the leading contribution of the first term, $\propto 1/x^s$, is provided by the first term in the brackets, we obtain the following equation:

$$-(1 + \eta_e)\frac{c}{x^s} + c\int_{x+\ln 2}^{x_{\rm att}} \left[1 - \frac{1}{e^{x'-x} - 1} + \frac{1}{(e^{x'-x} - 1)^2}\right]\frac{dx'}{x'^{1+s}} + 1 = 0, \tag{C5}$$

with $x_{\rm att} = \ln\tilde{\varepsilon}_{\rm att}$. The integral term yields $(c/s)(1/x^s - 1/x_{\rm att}^s) + O(1/x^{1+s})$. We see that Equation (C5) is satisfied for $s = (1 + \eta_e)^{-1}$ and $c = sx_{\rm att}^s$, which gives us Equation (28).

One can also roughly estimate the form of electron spectrum at $\tilde{\varepsilon} \lesssim \eta_p \ln\tilde{\varepsilon}_{\rm att}$, still assuming $\tilde{\varepsilon} \gg 1$. In this case, the primary ionization in Equation (27) is dominated by the term $2\zeta_1/\tilde{\varepsilon}^3$. Keeping in mind that the above analysis is performed for the term $2\zeta_2/\tilde{\varepsilon}^2$, we conclude that the sought spectrum obeys Equation (C4) with the last term (unity) replaced by $1/\tilde{\varepsilon}$. One

can see that, up to a factor depending on $\ln\tilde{\varepsilon}$, the solution is given by the following leading term:

$$\tilde{F}(\varepsilon) \sim \frac{1}{2(1+\eta_e)\tilde{\varepsilon}^2}, \tag{C6}$$

where $\tilde{F} = (I/2\zeta_1)F$. This gives us Equation (29).

To include the contribution of excitation collisions to the high-energy solution, we take into account that cross sections for H_2 ionization and excitation (of singlet states) behave similarly at large ε (Dalgarno et al. 1999; Janev et al. 2003). This implies that the ratio $\sigma_{\mathrm{exc},k}/\sigma_{\mathrm{ion},e}$ tends to a constant as $\varepsilon \to \infty$. Then, expanding a difference of the excitation terms in Equation (27) and taking into account Equation (8) yields the following additional contribution to Equation (C4):

$$\frac{\eta_e}{2}[\tilde{\varepsilon}^2 \ln\tilde{\varepsilon}\ \tilde{F}'(\tilde{\varepsilon}) + \tilde{\varepsilon}\ \tilde{F}(\tilde{\varepsilon})] \sum_k \frac{\Delta_k}{I}\left(\frac{\sigma_{\mathrm{exc},k}}{\sigma_{\mathrm{ion},e}}\right)_\infty,$$

where the cross-sectional ratios are evaluated at $\varepsilon \to \infty$. Hence, the high-energy asymptote of Equation (28) is valid also in the presence of excitation collisions, where η_e should be replaced with the modified value η_e^* given by Equation (31).

Appendix D
Analytical Estimates of $\zeta_{\mathrm{sec}}/\zeta_{\mathrm{p}}$

The high-energy analytical spectrum of secondary electrons, given by Equations (28) and (29), allows us to qualitatively understand Figure 3.

For monoenergetic protons with $E = E_{\mathrm{att}}(N)$, the energy dependence of ζ_1 and ζ_2 can be approximated by step-functions, and $\zeta_p = [1 + \eta_p \ln(\tilde{\varepsilon}_{\mathrm{att}}/4)]\zeta_2$. Let us write ζ_{sec} as a sum $\zeta_{\mathrm{sec}\,1} + \zeta_{\mathrm{sec}\,2}$, representing contributions $F \propto \zeta_{1,2}$ to the integral in Equation (32). We calculate $\zeta_{\mathrm{sec}\,2}$ by substituting Equation (28) and integrating over $\tilde{\varepsilon}$ from $\eta_p \ln\tilde{\varepsilon}_{\mathrm{att}}$ to $\tilde{\varepsilon}_{\mathrm{att}}$; as Equation (28) gives the leading dependence on $\ln\tilde{\varepsilon}$, we keep only the leading term also in Equation (8) and substitute $\Phi(\varepsilon) \approx \frac{1}{2}\eta_e \ln\tilde{\varepsilon}$. This yields the asymptotic expression

$$\frac{\zeta_{\mathrm{sec}\,2}}{\zeta_p} \approx \frac{1}{\eta_p} - \frac{1}{\eta_p}\left(\frac{\ln\tilde{\varepsilon}_{\mathrm{att}}}{\ln\ln\tilde{\varepsilon}_{\mathrm{att}}}\right)^{-\frac{\eta_e}{1+\eta_e}}, \tag{D1}$$

which is formally valid for sufficiently large N and neglects further corrections depending on $\ln\ln\tilde{\varepsilon}_{\mathrm{att}}$. Regarding $\zeta_{\mathrm{sec}\,1}$, Equation (29) is too crude to obtain a quantitative estimate. Nevertheless, it allows us to understand how $\zeta_{\mathrm{sec}\,1}$ depends on $\varepsilon_{\mathrm{att}}$. For large $\tilde{\varepsilon}_{\mathrm{att}}$, one can write $\zeta_1 \approx \zeta_p$. Substituting Equation (29) and $\Phi(\varepsilon)$ determined by Equation (8) into Equation (32) and integrating from $\sim$1 to $\sim\ln\tilde{\varepsilon}_{\mathrm{att}}$ gives

$$\frac{\zeta_{\mathrm{sec}\,1}}{\zeta_p} \sim \mathrm{const} - \frac{1}{\ln\tilde{\varepsilon}_{\mathrm{att}}}, \tag{D2}$$

with const ≈ 0.4. The logarithmic dependence of the integrand on ε, omitted to derive Equation (D2), results in terms $\ln\ln\tilde{\varepsilon}_{\mathrm{att}}$. The convergence of Equation (D2) to a constant at $N \to \infty$ is substantially faster than that of Equation (D1), and therefore the latter determines the behavior of $\zeta_{\mathrm{sec}}/\zeta_p$ at large N.

We note that the asymptotic convergence of $\zeta_{\mathrm{sec}}/\zeta_p$ is very slow—it actually occurs at unphysically large column densities (of $\gtrsim 10^{30}\,\mathrm{cm}^{-2}$). Hence, Equation (D1) merely serves as an indicator that $\zeta_{\mathrm{sec}}/\zeta_p$ keeps increasing at any relevant N.

Appendix E
Monte Carlo Simulations for Monoenergetic Protons

Using a step-function model for $\zeta_{1,2}$—which assumes that the primary ionization at a given N is produced by protons with the energy $E_{\mathrm{att}}(N)$—enables an easy comparison with direct simulations of the secondary ionization. The simulation algorithm is as follows: The first-generation secondary electron acquires the energy ε_1 in the range from 0 to $4(m_e/m_p)E_{\mathrm{att}}(N) - I$, with the probability given by Equation (1). Then, if that electron has energy greater than I, it creates the second-generation secondary electron with the energy ε_2 in the range from 0 to $\frac{1}{2}(\varepsilon_1 - I)$, with the probability given by Equation (2). Simultaneously, the energy of the first-generation electron is reduced from ε_1 to $\varepsilon_1 - \varepsilon_2 - I$. This process is repeated with all electrons with energy greater than I until there are none remaining. Then $\zeta_{\mathrm{sec}}/\zeta_p$ is equal to the average number of electrons in the simulation minus one, obtained after averaging over 10^9 primary ionizations.

Appendix F
Effect of Heavier CR Nuclei

Let us denote by $\mathcal{R}(N)$ a dependence $\zeta_{\mathrm{sec}}/\zeta_p$ versus N due to CR protons (one of the curves depicted in Figure 3). As explained in Section 6, the corresponding dependence for heavier nuclei k, with the atomic number Z_k and mass number A_k, is given by $\zeta_{\mathrm{sec}}^{(k)}/\zeta_p^{(k)} = \mathcal{R}(\psi_k N)$, where

$$\psi_k = Z_k^2/A_k, \tag{F1}$$

is unity for ^{4}He and > 1 for other stable nuclei. Our aim is to calculate the ratio of the total secondary ionization rate, $\zeta_{\mathrm{sec}}^{\Sigma} = \zeta_{\mathrm{sec}} + \sum_k \zeta_{\mathrm{sec}}^{(k)}$, to the total primary rate, $\zeta_p^{\Sigma} = \zeta_p + \sum_k \zeta_p^{(k)}$. Simple manipulation yields

$$\frac{\zeta_{\mathrm{sec}}^{\Sigma}}{\zeta_p^{\Sigma}} = \mathcal{R}(N)\ \frac{1 + \sum_k \frac{\mathcal{R}(\psi_k N)}{\mathcal{R}(N)}\frac{\zeta_p^{(k)}}{\zeta_p}}{1 + \sum_k \frac{\zeta_p^{(k)}}{\zeta_p}}. \tag{F2}$$

The ratio of the primary ionization rates, $\zeta_p^{(k)}/\zeta_p$, is evaluated by employing the dependence $\zeta_p(N) \propto N^{-\alpha}$ with $\alpha = \frac{a+d-1}{1+d}$, derived for a power-law interstellar spectrum of protons by Silsbee & Ivlev (2019; see also Appendix B). Given that the attenuation energy (per nucleon) of nucleus k is $E_{\mathrm{att}}(\psi_k N)$ and that their ionization rate is proportional to $Z_k^2 \equiv A_k \psi_k$, we obtain

$$\frac{\zeta_p^{(k)}}{\zeta_p} = x_k A_k \psi_k^{1-\alpha}, \tag{F3}$$

where x_k is the interstellar abundance relative to protons.

Equation (F2) shows that the effect of heavier nuclei is to increase the relative magnitude of the secondary ionization, because $\mathcal{R}(N)$ is an increasing function. However, the magnitude of the effect is negligible. Assuming an interstellar spectrum $\mathscr{H}$ with $a = 0.8$, which gives $\alpha \approx 0.35$, and using galactic CR abundances estimated from Dartois et al. (2015), we conclude that the fraction factor on the rhs of Equation (F2) differs form unity by less than 1%.

ORCID iDs

Alexei V. Ivlev https://orcid.org/0000-0002-1590-1018
Kedron Silsbee https://orcid.org/0000-0003-1572-0505
Marco Padovani https://orcid.org/0000-0003-2303-0096

References

Bethe, H. 1930, AnP, 397, 325
Caselli, P., & Ceccarelli, C. 2012, A&ARv, 20, 56
Caselli, P., Walmsley, C. M., Terzieva, R., & Herbst, E. 1998, ApJ, 499, 234
Cecchi-Pestellini, C., & Aiello, S. 1992, MNRAS, 258, 125
Cravens, T. E., & Dalgarno, A. 1978, ApJ, 219, 750
Cummings, A. C., Stone, E. C., Heikkila, B. C., et al. 2016, ApJ, 831, 18
Dalgarno, A., & Griffing, G. W. 1958, RSPSA, 248, 415
Dalgarno, A., Yan, M., & Liu, W. 1999, ApJS, 125, 237
Dartois, E., Augé, B., Rothard, H., et al. 2015, NIMPB, 365, 472
Erskine, G. A. 1954, RSPSA, 224, 362
Fano, U. 1953, PhRv, 92, 328
Galli, D., Walmsley, M., & Gonçalves, J. 2002, A&A, 394, 275
Glassgold, A. E., Galli, D., & Padovani, M. 2012, ApJ, 756, 157
Glassgold, A. E., & Langer, W. D. 1973, ApJ, 186, 859
Indriolo, N., & McCall, B. J. 2012, ApJ, 745, 91
Ivlev, A. V., Silsbee, K., Sipilä, O., & Caselli, P. 2019, ApJ, 884, 176
Janev, R. K., Reiter, D., & Samm, U. 2003, Collision Processes in Low-Temperature Hydrogen Plasmas (Jülich: Forschungszentrum, Zentralbibliothek)
Keto, E., & Caselli, P. 2008, ApJ, 683, 238
Keto, E., Rawlings, J., & Caselli, P. 2014, MNRAS, 440, 2616
Kim, Y.-K., & Rudd, M. E. 1994, PhRvA, 50, 3954
Kim, Y.-K., Santos, J. P., & Parente, F. 2000, PhRvA, 62, 052710
Knipp, J. K., Eguchi, T., Ohta, M., & Nagata, S. 1953, PThPh, 10, 24
Landau, L., & Lifshitz, E. 1991, Quantum Mechanics: Non-Relativistic Theory (Oxford: Pergamon)
McKee, C. F. 1989, ApJ, 345, 782
Mott, N. F. 1930, RSPSA, 126, 259
Neufeld, D. A., & Wolfire, M. G. 2017, ApJ, 845, 163
Padovani, M., Galli, D., Ivlev, A. V., Caselli, P., & Ferrara, A. 2018a, A&A, 619, A144
Padovani, M., Ivlev, A. V., Galli, D., et al. 2020, SSRv, 216, 29
Padovani, M., Ivlev, A. V., Galli, D., & Caselli, P. 2018b, A&A, 614, A111
Prasad, S. S., & Tarafdar, S. P. 1983, ApJ, 267, 603
Rudd, M. E. 1987, RadR, 109, 1
Rudd, M. E. 1988, PhRvA, 38, 6129
Rudd, M. E., Kim, Y. K., Madison, D. H., & Gay, T. J. 1992, RvMP, 64, 441
Shu, F. H., Adams, F. C., & Lizano, S. 1987, ARA&A, 25, 23
Silsbee, K., & Ivlev, A. V. 2019, ApJ, 879, 14
Spencer, L. V., & Fano, U. 1954, PhRv, 93, 1172
Spitzer, L. J., & Tomasko, M. G. 1968, ApJ, 152, 971
Wilms, J., Allen, A., & McCray, R. 2000, ApJ, 542, 914
Xu, Y., & McCray, R. 1991, ApJ, 375, 190
Zhao, B., Caselli, P., Li, Z.-Y., et al. 2016, MNRAS, 460, 2050
Zhao, B., Caselli, P., Li, Z.-Y., & Krasnopolsky, R. 2018, MNRAS, 473, 4868